Chapter Three

Thermodynamics of the Acicular Ferrite Transformation

3.1 Introduction

Acicular ferrite (α_a) is a phase formed by the transformation of austenite (γ) during cooling of low-alloy steel weld deposits [1,162]. It forms in a temperature range where diffusional transformations become relatively sluggish [1] and give way to displacive products such as Widmanstätten ferrite, bainite and martensite. Its morphology consists of non-parallel plates of ferrite, which during the early stages of transformation nucleate on inclusions [60,61] present in the columnar austenite grains typical of weld deposits. Subsequent plates may nucleate sympathetically on these inclusion-nucleated plates [62], so that a one-to-one correspondence between the number of active-inclusions and the number of α_a plates is not expected. However, the mechanism by which acicular ferrite grows is not understood and this hinders the development of phase transformation models for predicting the microstructure of welds. The work below deals with experiments on the thermodynamics of the formation of acicular ferrite from austenite.

The term "acicular" means "shaped and pointed like a needle" but it is generally recognised that α_a has in three-dimensions the morphology of thin-plates. In wrought steels, the formation of plate-shaped ferrite (whether it be bainite or Widmanstätten ferrite) is always accompanied by a change in the shape of the transformed region [48,89,100]. This shape change can be described as an invariant-plane strain with a significant shear component [89,100] and is generally taken to imply a displacive transformation mechanism [51] and the existence of an atomic correspondence between the parent and product phases, at least as far as atoms in the substitutional sites are concerned. Interstitial atoms, such as carbon may diffuse during transformation (especially when the ferrite forms at low-under-coolings where the partitioning of carbon is a thermodynamic necessity), without affecting the shape change or the displacive character of the transformation [25,163]. The shape change accompanying the transformation of acicular ferrite (α_a) has been determined experimentally [65]. Acicular ferrite may in fact be bainite or intragranularly nucleated Widmanstätten ferrite, but its transformation mechanism is not at all established.

The classification of microstructures on the basis of morphology is of considerable use in the study of structure-property relationships, but the prediction of microstructure requires a deeper understanding of the transformation mechanism. It is now well established [53-55] that the presence of acicular ferrite in the primary microstructure of

low-alloy steel weld deposits leads to improved toughness, but the mechanism of its formation is not understood. Attempts at modelling the primary microstructure thus rely on deducing the acicular ferrite content by difference rather than by direct prediction [1]. In this work, the aim was to deduce fundamental information about the growth of acicular ferrite, focussing on whether the growth is diffusionless.

3.2 Experimental Method

To enable the study of acicular ferrite without substantial interference from other reactions, a high-hardenability manual metal arc weld was deposited at a speed of 2 mm/s, using a welding current and voltage of 180A and 23V (DC+) respectively. The joint geometry was compatible with ISO 2560, the weld consisting of 21 runs with 3 runs per layer, the interpass temperature being 250°C. The composition of the weld WB was found to be Fe-0.06C-0.27Si-1.84Mn-2.48Ni-0.2Mo (wt.%) and the deposit contained an oxygen level of 399ppm and a nitrogen level of 111ppm by wt. together with 0.01 Al, 0.02Ti and 0.01Nb wt%.

Specimens for dilatometric experiments were machined from the weld deposits, so that the cylinder axes were parallel to the welding direction. The specimens were machined from regions far from the parent plate and are not affected by dilution from the parent material. All experiments were conducted on specimens which had been homogenised at 1250°C for 3 days, while sealed in quartz tubes containing a partial pressure of pure argon. Finally, the specimens for dilatometry were in the form of 3mm diameter cylindrical rods with a 1.0mm diameter bore and a 20mm length, electroplated with about 0.08mm layer of nickel, to provide constraint and avoid surface nucleation or surface degradation effects. Nickel plating was carried out in two stages - striking and plating. Striking was carried out in a solution made up of 250g $NiSO_4$, 27ml conc. sulphuric acid, and water, amounting to 1 litre in all. The solution was used at 50°C, with a current density of 775mA/cm^2, for 3 minutes. The plating solution consisted of 140g$NiSO_4$, 140g Anhydrous Sodium Sulphate, 15g Ammonium Chloride and 20g Boric Acid, made up to 1 litre with distilled water. The plating was carried out at 50°C, with a current density of 40mA/cm^2, for 15 minutes.

All dilatometry was performed on a Theta Industries high-speed dilatometer, which has a water cooled radio-frequency furnace of essentially zero thermal mass, since it is only the specimen which undergoes the programmed thermal cycle. The length transducer on the dilatometer was calibrated using pure platinum and pure nickel specimens of known thermal expansion characteristics. This enables rapid heating or cooling experiments to be carried out. The dilatometer has been specially interfaced with a BBC/Acron

microcomputer so that length, time and temperature information can be recorded at microsecond intervals, and the data stored on a floppy disc. The information is then transferred to a mainframe IBM3081 computer for further analysis.

The specimens were austenitised at 950°C for 10 minutes (or 1200°C for 30 minutes) before helium gas quenching to the different isothermal transformation temperature (480, 460 and 440°C). The relative length change ($\Delta L/L$) during the isothermal transformation was measured and the corresponding relative length change versus time has been plotted. The carbon content of residual austenite when isothermal transformation ceases is very useful in understanding the transformation mechanism. The maximum relative length change (ΔL_m) can be converted into the volume fraction of ferrite transformed, from which the carbon content of the residual austenite can be calculated. The carbon content of the residual austenite as a function of the relative length change in isothermal transformation can be estimated from equation III.1 and III.2. The relative length change ($\Delta L/L$) corresponding to a volume fraction (V) of ferrite transformed is given [164] by:

$$\Delta L/L = [2V(a_\alpha^3) + (1-V)(a_\gamma^3) - \bar{a}_\gamma^3]/[3\bar{a}_\gamma^3] \qquad \text{(III.1)}$$

where a_α = lattice parameter of ferrite at the reaction temperature,

$\bar{a}_\gamma$ = lattice parameter of austenite at the beginning of the isothermal transformation

a_γ = lattice parameter of austenite at any stage of the isothermal transformation.

$$a_\alpha = \bar{a}_\alpha[1 + e_\alpha(T-293)]$$

where $\bar{a}_\alpha$ = lattice parameter of ferrite, at ambient temperature (293K) measured by X-ray diffraction,

e_α = linear expansion coefficient of ferrite.

$$\bar{a}_\gamma = (a_0 + \Sigma CiXi)\,[1 + e_\gamma(T-293)]$$

where a_0 = lattice parameter of unalloyed austenite,

Xi = concentration of alloying element i,

Ci = coefficients (obtained from Reference 165) relating Xi to the change in a_0. Suppose C_1 for carbon, C_2,C_3 C_4, ... for other substitutional alloy elements.

e_γ = linear expansion coefficient of austenite.

Hence $\bar{a}_\gamma = (a_0 + C_1\bar{X} + C_2X_2\ C_3X_3 + C_4X_4 + \ldots)[1 + e_\gamma(T-293)]$,

and $a_\gamma = (a_0 + C_1X_\gamma + C_2X_2 + C_3X_3 + C_4C_4 + \ldots)[1 + e_\gamma(T-293)]$

where $\bar{X}$ = average carbon concentration of alloy,

X_γ = carbon concentration of residual austenite.

After ferrite formation, the carbon is rejected from ferrite to residual austenite; therefore

$$X_\gamma = \bar{X} + [V(\bar{X} - S)/(1-V)] \quad \text{(III.2)}$$

where S = amount of carbon locked up in ferrite either as carbides or in solution.

All the concentrations used in the calculation of equation III.1 and III.2 are in wt%. The calculations also require the linear expansion coefficients of austenite and ferrite. The ferrite linear expansion coefficient e_α was determined by first tempering a specimen at 600°C for 10 minutes to decompose any retained austenite and then recording the length change during cooling at a rate of 0.063°C/s. The measurements do not therefore account for the presence of a very small amount of carbide. The graph of relative length versus temperature is plotted in Figure III.1, from which the linear expansion coefficient of ferrite was obtained ($e_\alpha = 1.15 \times 10^{-5}k^{-1}$). The γ expansion coefficient was measured while specimen was in the γ single-phase field, as shown in Figure III.2 ($e_\gamma = 1.769 \times 10^{-5}k^{-1}$). The ferrite lattice parameter ($\bar{a}_\alpha$) at ambient temperature was measured using a Debye-Scherrer technique. The testing specimen had been annealed at 600°C for 1 hour, while sealed in quartz tubes containing a partial pressure of pure argon, and then machined to the form of 0.5mm x 0.5mm x 15mm wire. Finally the specimen was chemically polished in a solution made up of 5% HF, 50% H_2O_2 and 45% H_2O for one minute to remove the deformation layer before testing. In the X-ray lattice parameter measurement, the CuK_α radiation and a standard Debye camera were used. The wave length of CuK_α radiation is 1.5417Å, and the Diameter of the standard Debye camera is 114.60mm. Newton-Ralphson extrapolation [166], using 011, 002, 112, 022, 013 lines, was used to obtain the ambient temperature ferrite lattice parameter $\bar{a}_\alpha = 2.8723$Å as shown in Figure III.3. This parameter differs by only 0.1% from that calculated using data from Reference 167. Using these values and making the appropriate substitution in equation III.1 and III.2, the carbon content of residual austenite X_γ values (Table III.1) are obtained using a computer programme. Since carbide precipitation does not occur rapidly over the time scale of the experiments, S in equation III.2 is taken to be 0.02 wt%, which is approximately the maximum solubility of carbon in ferrite.

3.3 Results and Discussion

The primary as-deposited microstructure of weld metal WB studied in this investigation has been shown in Figure II.6c. It consists chiefly of acicular ferrite, with a small amount of allotriomorphic ferrite, Widmanstätten ferrite and microphases. The calculated TTT curve for the weld metal has also been shown in Figure II.1a. In this alloy, the Widmanstätten ferrite start temperature (W_S) and bainite start temperature (B_S) have been calculated, and it has been found that $W_S = B_S = 500$°C. This means [100] that

Widmanstätten ferrite should not be observed at all and immediately implies that the acicular ferrite observed in the weld deposit is likely to be bainite if it is not a completely new transformation. Figure II.1a also shows that for any reasonable weld cooling rate, the cooling curve cannot intersect the upper C curve (diffusional C curve), so that the alloy can only transform by a displacive mechanism. The alloy is therefore ideally suited to avoid interference from other transformation products during the study of acicular ferrite. In addition, transformation during the quench to the isothermal transformation temperature can easily be avoided. Certainly, a weld deposit is necessarily chemically inhomogeneous, and some formation of allotriomorphic ferrite and Widmanstätten ferrite cannot thus be avoided in the solute depleted regions, as seen in Figure II.6c.

3.3.1 Grain Size Effect

The problem of resolving the nature of acicular ferrite is made worse by the fact that it does not readily occur in wrought steels, due to the absence intragranular heterogeneous nucleation sites and because the austenite grain size of such steels is deliberately kept small; transformations initiated at austenite grain boundaries thus swamp the interior regions as well. However, if after deposition, a weld is reheated into the austenite phase field to generate large austenite grains then these new grains still contain the inclusions which were present in the original deposit. Isothermal transformation of this structure in a temperature range where acicular ferrite usually forms in welds should then lead to the intragranular nucleation and growth of plates whose morphology should be identical to that of the acicular ferrite observed in weld deposits.

The austenite grain sizes for the homogenised specimen austenitised at 950°C for 10 minutes, and at 1200°C for 30 minutes have been investigated. The heat treatment processes were carried out in dilatometer as well. After austenitisation, the specimens were quenched by helium jets and then tempered at 600°C for 1 hour in order to reveal the austenite grain boundaries as shown in Figure III.4. Figure III.4a displays the smaller austenite grain for the specimen austenitised at 950°C for 10 minutes. Figure III.4b presents larger austenite grain for the specimen austenite at 1200°C for 30 minutes. Using linear intercept method, the austenite grains were measured on Quantimet 720 image analysing computer. The average grain size for the former is about 15μm, and for the latter about 45μm. The higher austenitisation temperature has clearly led to a larger austenite grain size. The results of isothermal transformation experiments on reheated weld metal are illustrated in Figure III.5, 6, 7 and 8. The optical micrograph (Figure III.5a) shows some ferrite plates forming after austenitisation of weld metal at 950°C for 10 minutes followed by isothermal transformation at 490°C for 30 minutes prior to quenching to ambient temperature. It is noted that the ferrite plates grow from austenite

grain boundaries and adjacent ferrite plates are parallel to each other. This is the feature of bainitic ferrite. It is also found that the transformation temperature 490°C is very close to the B_S temperature (the calculated B_S temperature is 500°C). Figure III.5b also displays some ferrite plates obtained after austenitisation of weld metal at 1200°C for 30 minutes followed by isothermal transformation at 490°C for 30 minutes. The ferrite plates seem to be scattered in the austenitic matrix (now martensite after quenching to room temperature). It is also noted that the major ferrite plates are not parallel with their adjacent plates. The morphology is like that of acicular ferrite. Figure III.6 demonstrates the results of isothermal transformation at 460°C for 30 minutes; in one case the weld was reaustenitised at 950°C for 10 minutes (Figure III.6a) and another sample was austenitised at 1200°C for 30 minutes (Figure III.6b) before isothermal transformation. It is clear (Figure III.6b) that isothermal transformation with the larger austenite grain condition has led to the intragranular nucleation of plates of ferrite which can be identified morphologically with acicular ferrite found in welds. On the other hand, in the specimen reaustenitised at 950°C, the small austenite grain size has prevented intragranular nucleation, the ferrite plate nucleation at the austenite grain boundaries and growing by a sub-unit mechanism to give the morphology of sheaves of upper bainite (Figure III.6a). The striking transmission electron micrographs in Figure III.7a and b distinctly confirm the morphologies of upper bainite and acicular ferrite in weld metal for the corresponding optical micrographs shown in Figure III.6a and b. In order to investigate the morphologies for higher volume fraction of bainite and acicular ferrite in weld metal, the isothermal transformation was carried out at 440°C for 30 minutes. The results are shown in Figure III.8. Figure III.8a displays large amount of bainite obtained after austenitisation of weld metal at 950°C for 10 minutes followed by isothermal transformation at 440°C for 30 minutes. The micrograph clearly demonstrates that the sheaves of bainite ferrite grow from grain boundaries, swamp the interior region of austenite grains, and them impinge with the opposite austenite grain boundaries. Figure III.8b shows a high volume fraction of acicular ferrite obtained after austenitisation at 1200°C for 30 minutes followed by isothermal transformation at 440°C for 30 minutes. The optical micrograph shows the interlocking nature of acicular ferrite because acicular ferrite nucleates intragranularly at inclusions within large austenite grains, and because of hard impingement between plates nucleated on adjacent inclusions. It is clear that acicular ferrite requires the presence of inclusions to initiate intragranular nucleation, and will only form when the austenite grain size is relatively large, so that events originated from the grain boundaries do not swamp those occurring intragranularly.

3.3.2 The Carbon Content of Residual Austenite

A further experiment is needed to clearly establish that acicular ferrite is similar to bainite and not to intragranularly nucleated Widmanstätten ferrite. Both bainite (α_b) and Widmanstätten ferrite (α_w) grow by a displacive transformation mechanism [25,89,100]. However, the formation of Widmanstätten ferrite involves the redistribution of carbon between the parent and product phases, but bainite initially forms by a diffusionless mechanism and the carbon later partitions into the remaining austenite [25,89,100]. This difference can be exploited to deduce whether acicular ferrite grows like conventional bainite or like Widmanstätten ferrite.

Considering first the diffusionless formation of bainite, the reaction should go to completion since there is no diffusion necessary. In practice, the whole of the austenite grain does not transform instantaneously because of kinetic restrictions (e.g. heterogeneous nucleation); even if the first plate forms without diffusion, it has a opportunity to reject its excess carbon into the residual austenite. Any further increment of transformation is therefore associated with a lower free energy change, due to the higher carbon content of the austenite from which it has to form. Eventually, a stage is reached where the transformation becomes thermodynamically impossible since the free energies of residual austenite and bainitic ferrite of the same composition become identical [25,89,100], as shown in Figure III.9. The locus of such positions, as a function of isothermal transformation temperature defines the T_0' curve [89,100], where austenite and bainite (with a certain amount of stored energy associated with transformation strains) of the same composition have equal free energies. The corresponding curve for stress-free austenite and ferrite of identical composition is conventionally called T_0 [104]. The bainite reaction should therefore stop when the carbon concentration of austenite (X_γ) reaches the level given by the T_0' for the isothermal transformation temperature concerned [100].

The Ae_3' curve (as shown in Figure III.9) may similarly be defined for the growth of Widmanstätten ferrite [100] which involves the paraequilibrium transformation with the partitioning of carbon. If the small amount of strain energy associated with the back-to-back formation of mutually accommodating plates of Widmanstätten ferrite is ignored, the Widmanstätten reaction should stop when X_γ reaches the level given by the Ae_3' curve for the isothermal transformation temperature concerned [100]. For any given Temperature, the carbon concentration given by Ae_3' curve is much larger than that given by the T_0' curve, so that a measurement of X_γ at reaction termination can clearly distinguish between Widmanstätten ferrite and bainite. Hence, the aim was to transform a weld metal isothermally in a temperature range where it is known to transform to just acicular ferrite,

and by studying the maximum extent of transformation in terms of the above criteria, to decide whether acicular ferrite resembles Widmanstätten ferrite or bainite with respect to its growth mechanism.

3.3.3 Dilatometry and Thermodynamic Analysis

The dilatometric specimens were austenitised at 950°C for 10 minutes or at 1200°C for 30 minutes before quenching to the isothermal transformation temperatures 440, 460 and 490°C. The isothermal transformation curves are presented in Figure III.10 and are seen to have a classical sigmoidal shape, with a rapid initial reaction. It is immediately apparent that the maximum degree of transformation at any temperature increases as temperature below the bainite start temperature (B_S = 500°C), showing that the weld metal exhibits the classical "incomplete reaction phenomenon" which is an identifying feature of bainitic transformation [25,89,100]. The carbon content of residual austenite X_γ corresponding to the maximum degree of transformation has been calculated, using equations III.1 and 2 and the following measurements: $e_\alpha = 1.150 \times 10^{-5}k^{-1}$, $e_\gamma = 1.769 \times 10^{-5}k^{-1}$, and the lattice parameter of ferrite in the weld, at ambient temperature. The carbon content of residual austenite (X_γ), the volume fraction of bainite (V_{α_b}) and the volume fraction of acicular ferrite (V_{α_a}) after complete isothermal transformation are shown in Table III.1. X_γ corresponding to the maximum degree of transformation is presented in Figure III.11, along with the relevant phase boundaries T'_0, T_0 and Ae'_3 (as calculated in Chapter Two). It is clear that acicular ferrite formation ceases at the T'_0 boundary, providing strong evidence that the formation of acicular ferrite is diffusionless, the redistribution of carbon into the residual austenite occurring at a stage after growth. The transformation mechanism of acicular ferrite is clearly established and is the same as that of bainite. The results also imply that the strain energy accompanying acicular ferrite growth is of the order of 400J/mol [100].

3.4 Conclusions

It is found that the formation of acicular ferrite at any particular transformation temperature ceases as the carbon concentration of the residual austenite reaches the T'_0 boundary, and that the transformation exhibits an "incomplete reaction phenomenon". The maximum extent of transformation increases with undercooling below the B_S temperature. These results provide strong evidence suggesting that the growth of acicular ferrite is diffusionless, with carbon partitioning into austenite after the transformation event. In this respect, acicular ferrite is identical to bainite. Evidence has also been provided to show that the morphology of acicular ferrite differs from that of bainite simply because the former nucleates intragranularly at inclusions within large austenite

grains and because of hard impingement between plates nucleated on adjacent inclusions. It is concluded that acicular ferrite is in fact bainite which nucleates intragranularly in the large austenite grains typical of weld deposits.

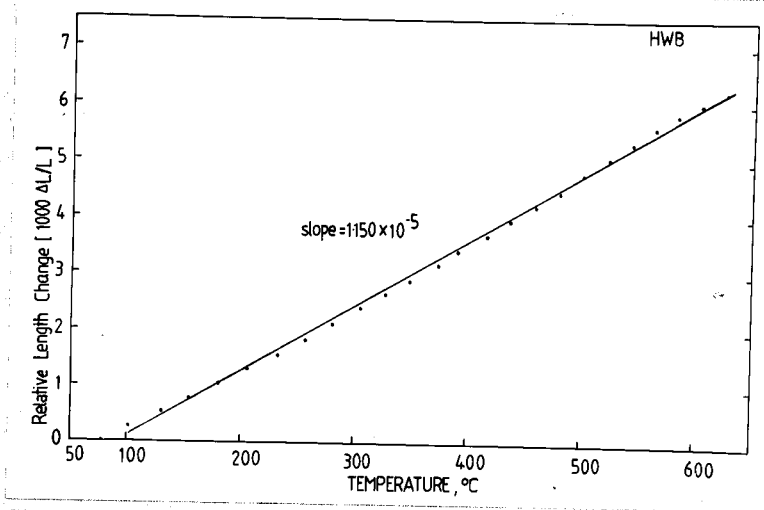

Fig. III.1 - Showing the graphs of relative length change versus temperature, from which the linear expansion coefficient of ferrite is obtained.

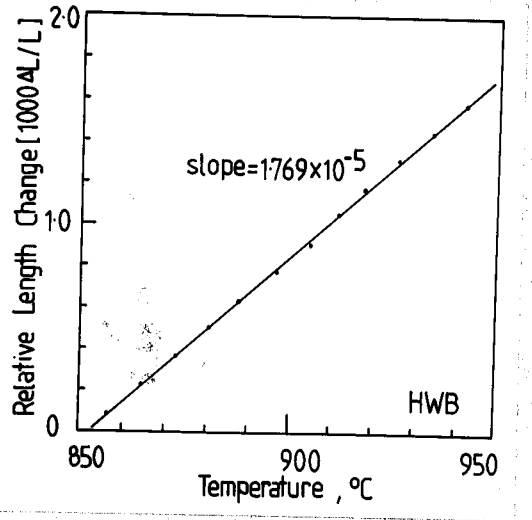

Fig. III.2 - Showing the graphs of relative length change versus temperature, from which the linear expansion coefficient of austenite is obtained.

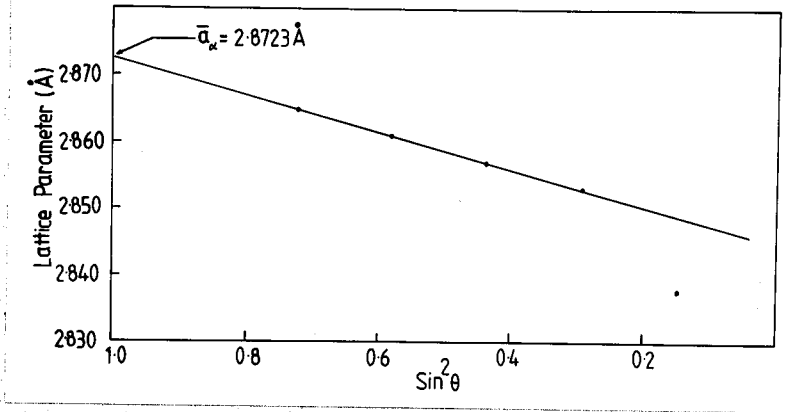

Fig. III.3 - Extrapolation of measured lattice parameter against $\sin^2\theta$. θ is the diffraction angle.

Fig. III.4a - Optical micrograph shows small austenite grains. Weld metal was reaustenitised at 950°C for 10 minutes and quenched by helium jets, and then tempered at 600°C for one hour.

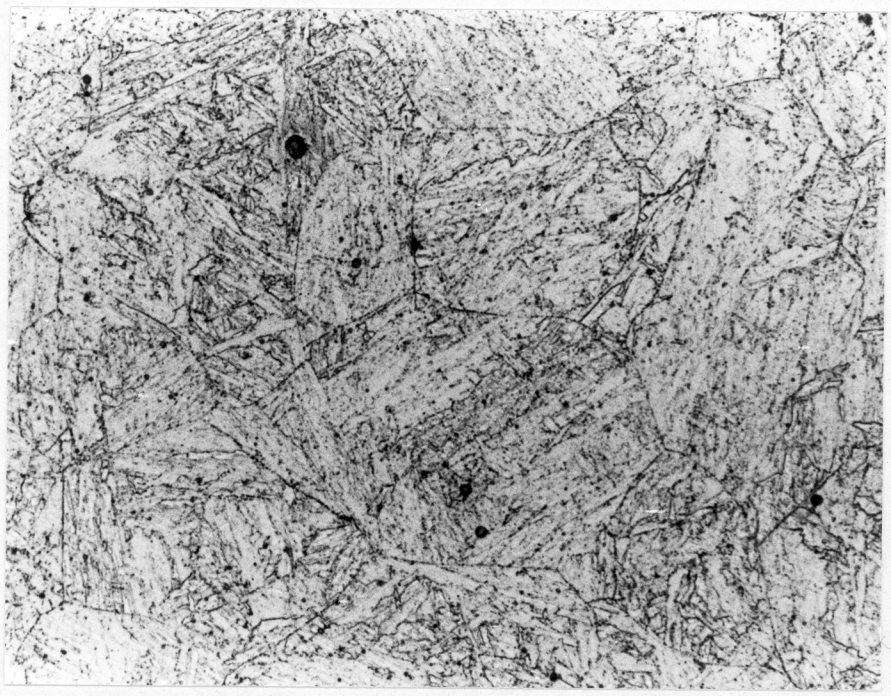

Fig. III.4b - Optical micrograph displays larger austenite grains. Weld metal was reaustenitised at 1200°C for 30 minutes and quenched by helium jets, and then tempered at 600°C for one hour.

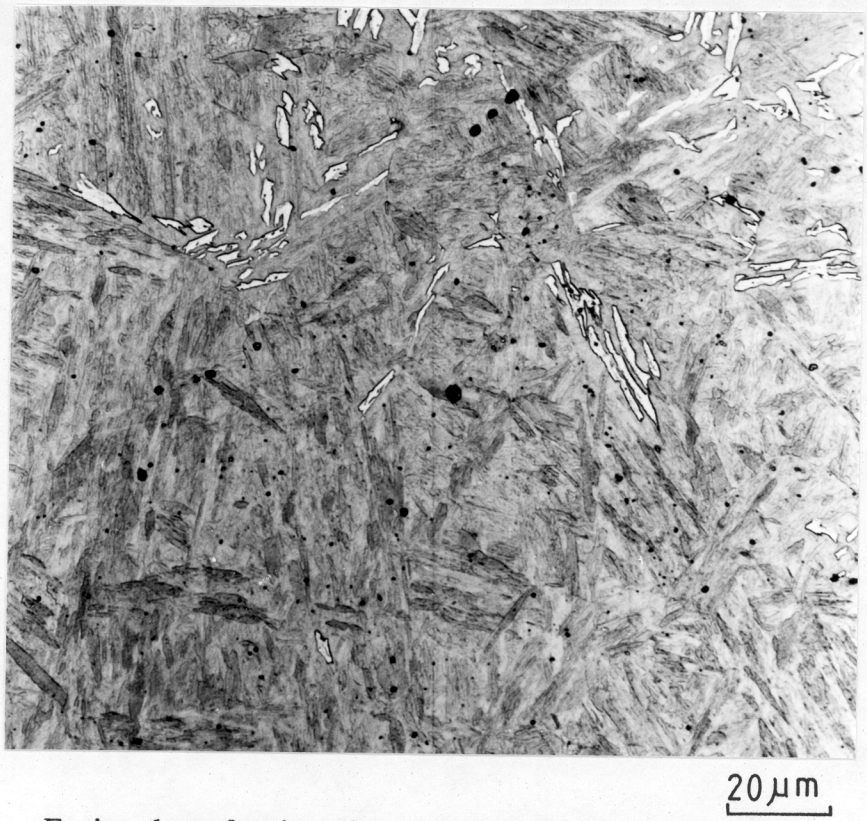

Fig. III.5a - Ferrite plates forming after austenitisation of weld metal at 950°C for 10 minutes followed by isothermal transformation at 490°C for 30 minutes.

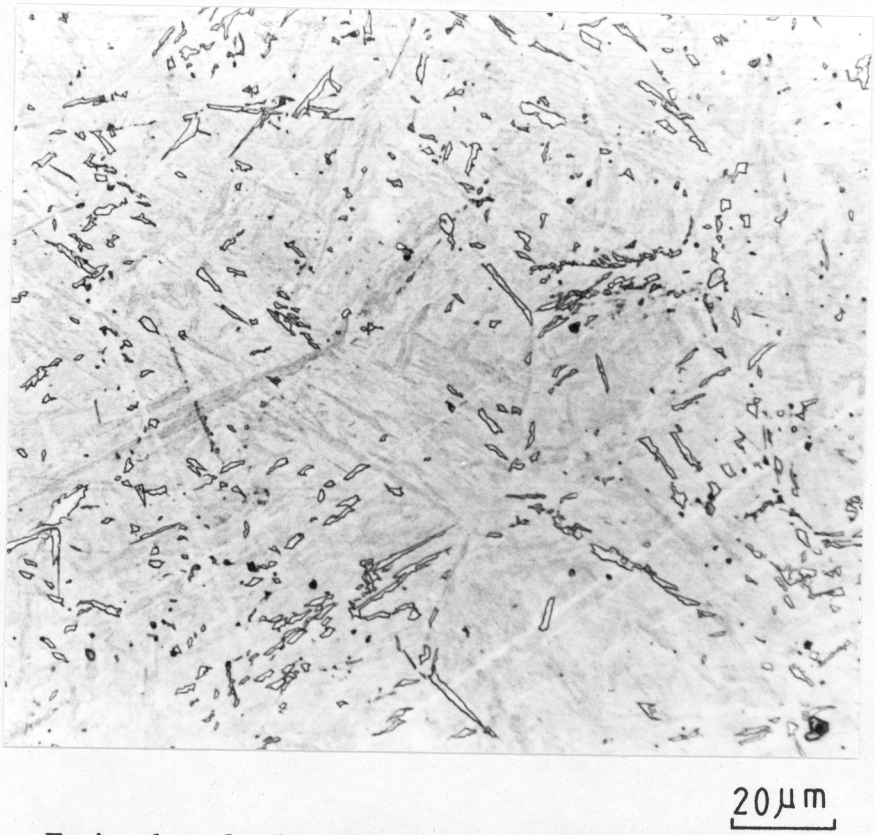

Fig. III.5b - Ferrite plates forming after austenitisation of weld metal at 1200°C for 30 minutes followed by isothermal transformation at 490°C for 30 minutes.

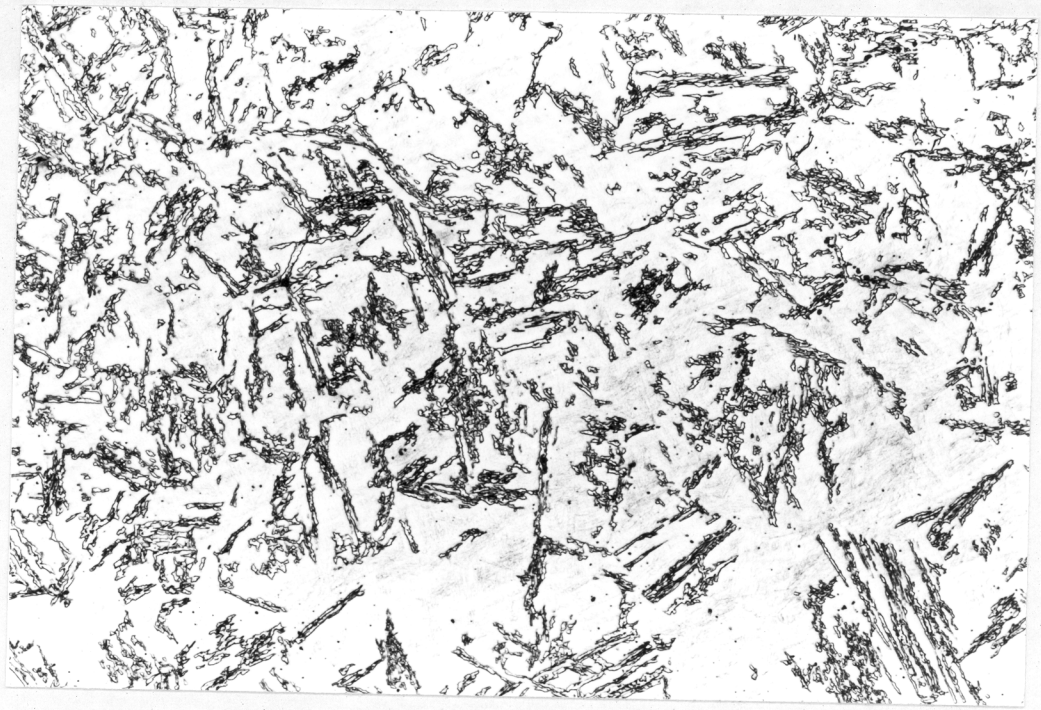

Fig. III.6a - Bainite obtained after austenitisation of weld metal at 950°C for 10 minutes followed by isothermal transformation at 460°C for 30 minutes.

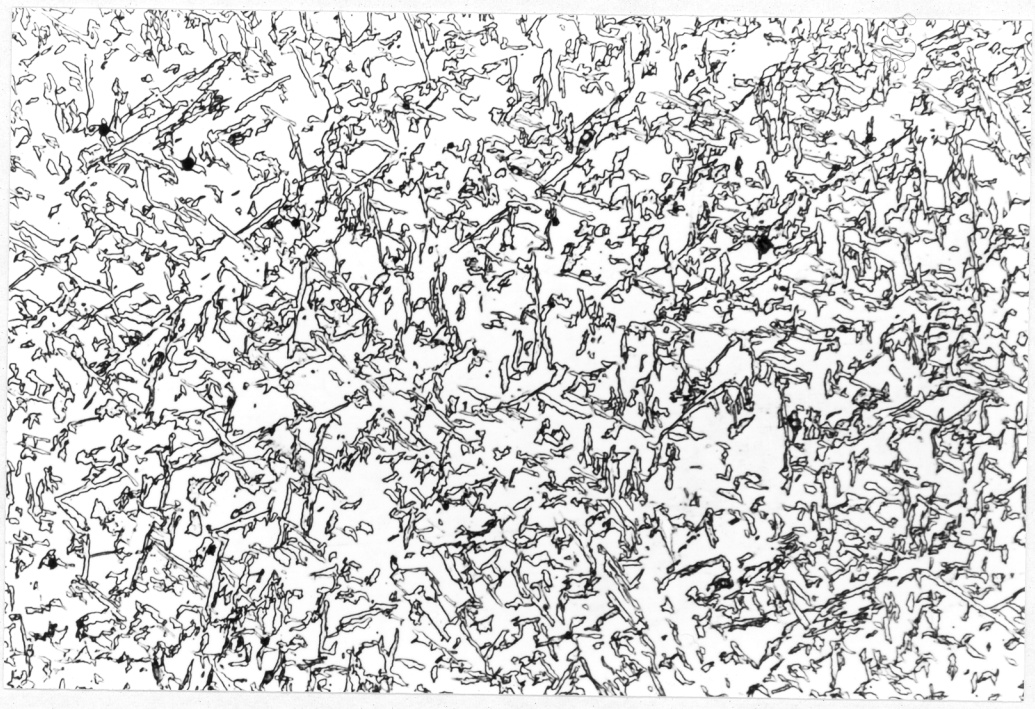

Fig. III.6b - Acicular ferrite obtained after austenitisation of weld metal at 1200°C for 30 minutes followed by isothermal transformation at 460°C for 30 minutes.

Fig. III.7a - Transmission electron micrograph shows classical sheaf of upper bainite. Weld metal was reaustenitised at 950°C for 10 minutes, isothermally transformed at 460°C for 30 minutes and then quenched by helium jets.

Fig. III.7b - Transmission electron micrograph shows acicular ferrite. Weld metal was reaustenitised at 1200°C for 30 minutes, followed by isothermal transformation at 460°C for 30 minutes and then quenched by helium jets.

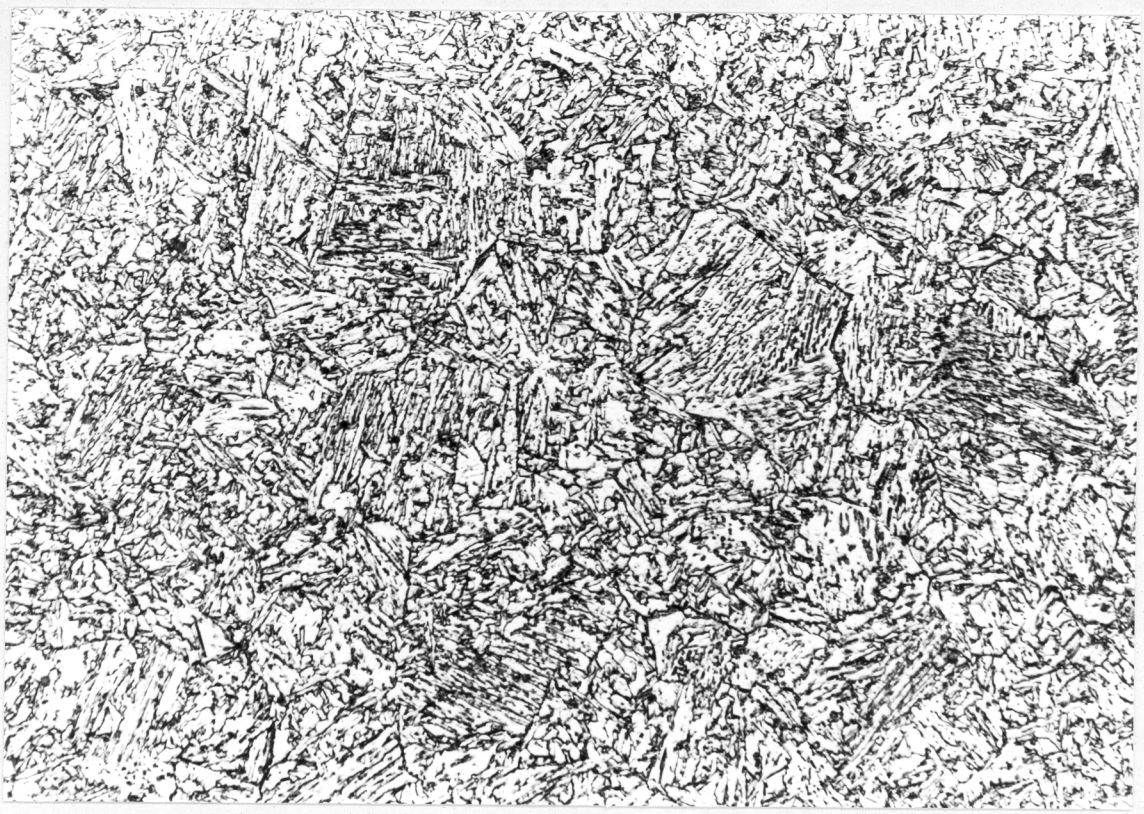

Fig. III.8a - High volume fraction of bainite obtained after austenitisation of weld metal at 950°C for 10 minutes followed by isothermal transformation at 440°C for 30 minutes.

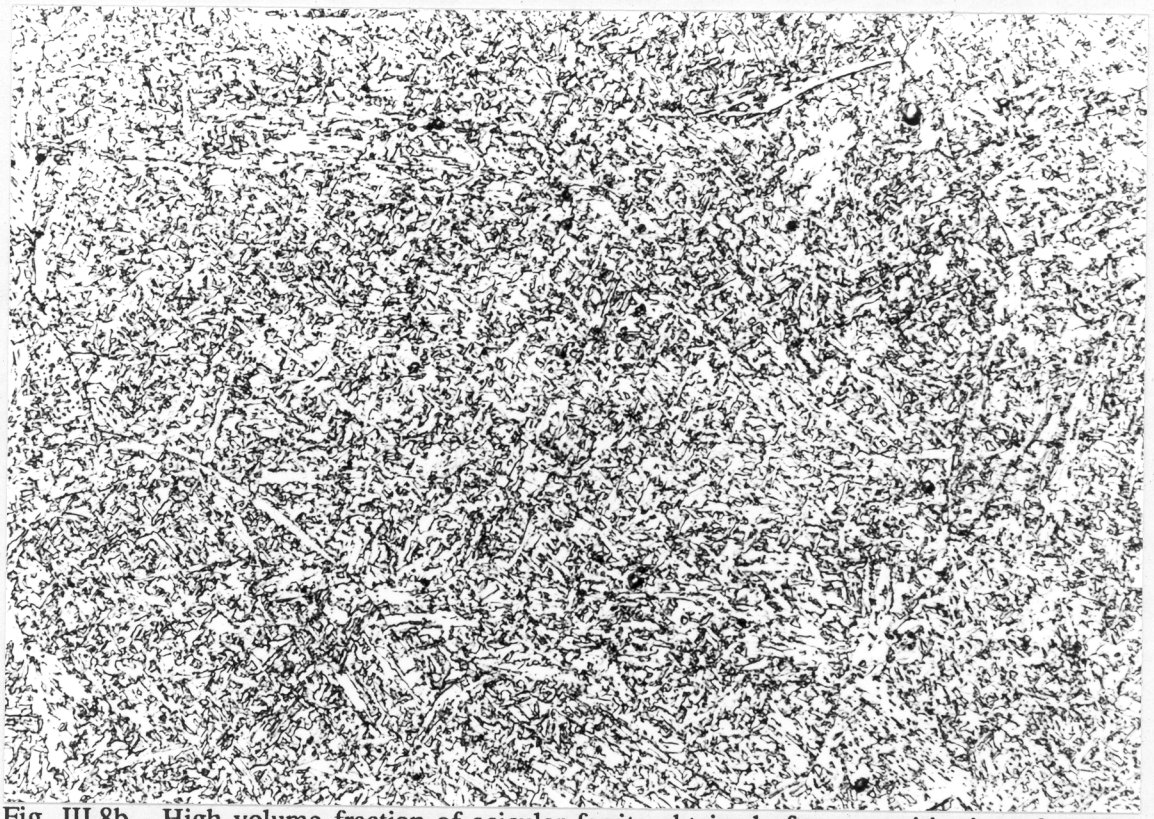

Fig. III.8b - High volume fraction of acicular ferrite obtained after austenitisation of weld metal at 1200°C for 30 minutes followed by isothermal transformation at 440°C for 30 minutes.

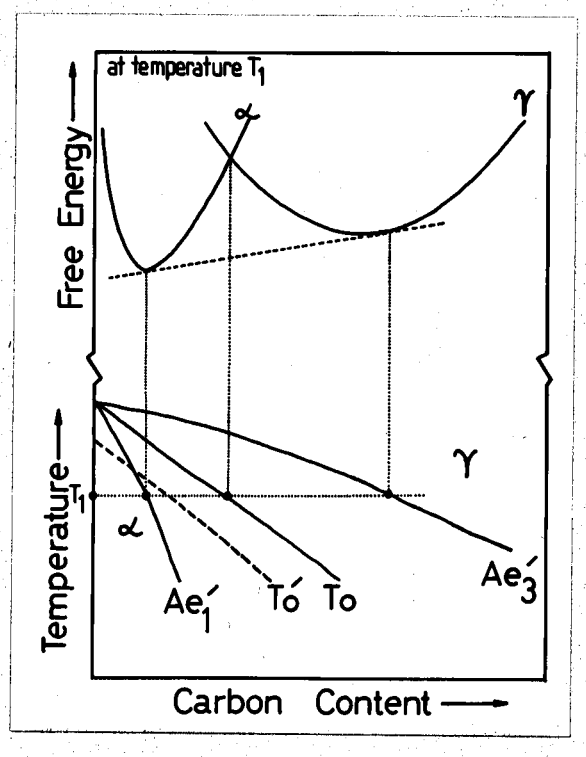

Fig. III.9 - Schematic diagram showing the construction of phase boundaries from free energy data. The T_0' line includes the effect of 400J/mol of strain energy due to transformation.

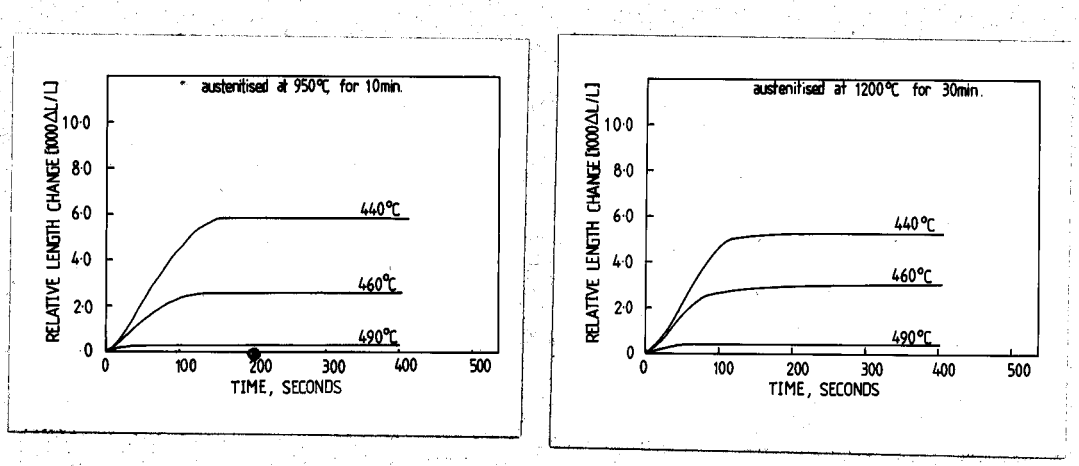

Fig. III.10 - (a) Isothermal transformation curves for weld reaustenitised at 950°C. (b) Isothermal transformation curves for weld reaustenitised at 1200°C.

Table III.1 - The carbon content of residual austenite (X_γ), the volume fraction of bainite (V_{α_b}) and the volume fraction of acicular ferrite (V_{α_a}) after isothermal transformation ceases.

isothermal transformation temperature (°C)	reaustenitisation at 950°C for 10 min. before isothermal transformation		reaustenitisation at 1200°C for 30 min. before isothermal transformation	
T_I	V_{α_b}	X_γ	V_{α_a}	X_γ
490	0.05	0.27×10^{-2}	0.08	0.28×10^{-2}
460	0.37	0.34×10^{-2}	0.40	0.35×10^{-2}
440	0.88	0.53×10^{-2}	0.86	0.50×10^{-2}

Note: X_γ in mol fraction.

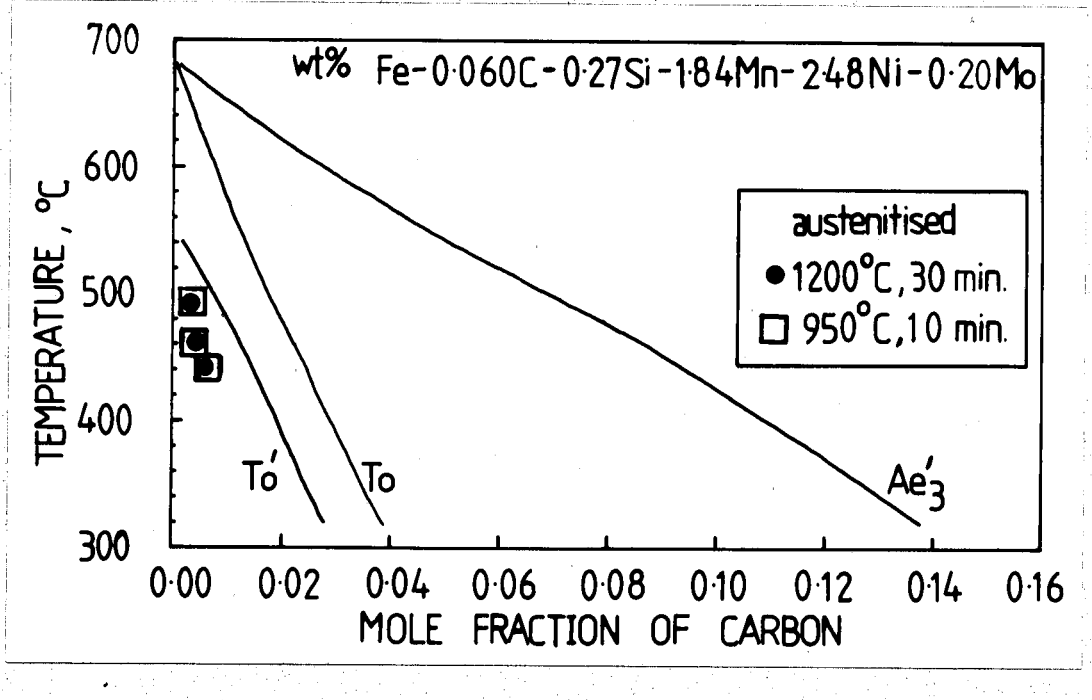

Fig. III.11 - Phase diagram, with experimental data on the carbon concentration of austenite at the termination of isothermal transformation. The reactions stop well before the Ae3' curves are reached.

Chapter Four

REAUSTENITISATION IN STEEL WELD DEPOSITS - PART 1

4.1 Introduction

Much work has recently been done on the prediction of the primary microstructure of fusion zone in weld deposits using detailed phase transformation theory, and this has met with reasonable success [1,31,77-79]. However, there is no corresponding theory available for the reheated microstructure, which can form a substantial proportion of a multipass weld deposit. The thermal cycle experienced in the reheated zone may just anneal the microstructure and cause recrystallisation and grain growth, or if the Ac_1 temperature is exceeded, it may reaustenitise to a degree depending on the thermodynamics and the kinetics of reaustenitisation. In order to establish a quantitative model for reaustenitisation in weld deposits, the work is initially limited to isothermal reaustenitisation experiments, and the starting microstructure is acicular ferrite (α_a) in a matrix of austenite, or bainite (α_b) in a matrix of austenite. The study of the overall transformation kinetics will be presented in Chapter Five.

The alloy HWB used in the investigation is a homogenised weld deposit of composition Fe-0.06C-0.27Si-1.84Mn-2.48Ni-0.20Mo-0.0040O-0.01Al-0.02Ti , wt%. The oxygen is tied up in the form of oxide inclusions. Alloy preparation and the experimental technique of dilatometry have been presented in Chapter Three. The same techniques of transmission microscopy and microanalysis have also been used as demonstrated in Chapter Two.

4.2 Isothermal Reaustenitisation

The aim was to study isothermal reaustenitisation, beginning with a microstructure consisting of bainite and austenite (or acicular ferrite and austenite). For this reason, the experiments were carried out on weld specimens homogenised, austenitised at 950°C for 10 minutes (or at 1200°C for 30 minutes), isothermally transformed to bainite (or acicular ferrite) at a temperature T_a = 460°C for 30 minutes (Figure III.6 and 7) and then rapidly up-quenched to a temperature T_γ for isothermal reaustenitisation. The specimens were not cooled below 460°C, in order to avoid the martensitic decomposition of some or all of the residual austenite at that temperature. It should be noted that 30 minutes at 460°C is more than adequate to allow the bainite (or acicular ferrite) transformation to terminate as shown in Figure III.10. It has also been demonstrated that for the alloy used, the bainite (or acicular ferrite) transformation ceases when the carbon content of residual austenite X_γ reaches the T_0' curve in Figure III.11. The precipitation of cementite (θ) from austenite is

very slow for this alloy, when compared with the time required for the α_b (or α_a) transformation to cease. For example, no cementite is found long after the completion of the bainite (or acicular ferrite) transformation at 460°C. Even when this mixture of bainitic ferrite and carbon-enriched residual austenite is annealed by raising the temperature to 600°C (directly from 460°C), cementite only precipitates from austenite after about 2 hours (as shown in Figure IV.1 including EDX data). Hence, cementite precipitation does not complicate the interpretation of the results, reaustenitisation being from a mixture of just bainitic ferrite (or acicular ferrite) and carbon-enriched austenite. The dilatometric output also showed (Figure IV.4a) that there was no decomposition of austenite during heating. In these circumstances, reaustenitisation involves just the growth of austenite and nucleation can be ignored.

4.2.1 Dilatometry

The results obtained from dilatometric experiments are presented in Figure IV.2 and 3. The first detectable growth of austenite was found to occur at T_γ = 680°C for both starting microstructures bainite plus austenite (Figure IV.2) and acicular ferrite plus austenite (Figure IV.3). In all cases the transformation rate was initially rapid, but decreased with time so that the specimen length eventually stopped changing, as transformation ceased. It should be noted that a small amount of transformation occurred during the up-quench, when attempts were made to isothermally reaustenitise specimens at temperatures above 725°C for both different starting microstructures. The transformation during the up-quench has been recorded by the computer; it contributes to specimen length change, and a correction for this has been made as shown in Figure IV.4. During continuous heating the specimens length varies linearly with temperature. Figure IV.4a shows the relative length change versus temperature curve for isothermal reaustenitisation at 715°C for 2 hours (from starting microstructure $\alpha_a+\gamma$), from which the maximum relative length change ΔL_m can be directly measured. In the case of higher temperature isothermal reaustenitisation, if the low-temperature part of the curve (in a relative length change versus temperature plot as shown in Figure IV.4b) is extrapolated to T_γ, the vertical difference between the extrapolated curve and the actual curve gives the relative length change ΔL_u due to transformation during the up-quench, which should be added to any relative length change ΔL_I due to isothermal transformation at T_γ. Therefore the maximum relative length change, $\Delta L_m = \Delta L_u + \Delta L_I$ as presented in Figure IV.4b.

The maximum relative length change (ΔL_m) versus the corresponding temperature of isothermal reaustenitisation (T_γ) is plotted in Figure IV.5. In the figure, the curves A and B show the experimental data for starting microstructures bainite plus austenite ($\alpha_b+\gamma$) and acicular ferrite plus austenite ($\alpha_a+\gamma$), respectively. The results are nearly the same,

and show that ΔL_m increases as T_γ increases from 680°C to 760°C and then stays essentially constant with further increase in T_γ. Since the temperature range covered is not very large, the results indicate that below 760°C, reaustenitisation is incomplete, the alloy becoming fully austenitic only above this temperature. Furthermore, the maximum degree of transformation to austenite increases from nearly zero at 680°C to complete reverse transformation at 760°C and above. It is also seen from Figures IV.2 and 3 that the rate of the reverse $\alpha \rightarrow \gamma$ transformation increases with T_γ for the starting microstructures $\alpha_b+\gamma$ and $\alpha_a+\gamma$.

4.2.2 Transmission Electron Microscopy

The transmission electron microscopy for isothermal reaustenitisation from starting microstructures bainite plus austenite, and acicular ferrite plus austenite has been studied as presented in Figure IV.6 and 7, respectively. Figure IV.6a shows micrograph for reaustenitisation at 680°C for 2 hours from starting microstructure $\alpha_b+\gamma$, in which the ferrite plates (original bainitic ferrite sub-units) are parallel to each other and are separated by the austenite layers (now become martensite after cooling to ambient temperature). The thickness of austenite layers does not seem to increase significantly because 680°C is the isothermal reaustenitisation starting temperature as expected from dilatometry. As the isothermal reaustenitisation temperature increases, the austenite layer becomes thicker. However the austenite layers still remain parallel with each other as shown in Figures IV.6b, c and d for reaustenitisation at 700°C, 720°C and 740°C for 2 hours. This provides strong evidence that austenite grows by the movement of the approximately planar γ/α interface. Figure IV.6e shows that there is some ferrite retained after reaustenitisation at 750°C for 2 hours. The electron micrograph in Figure IV.6f present complete martensite structure, which originally was full austenite at 760°C before quenching to room temperature (the helium gas quenching rate in dilatometer ≈ 60 °C/s). The electron microscopy for reaustenitisation from $\alpha_b+\gamma$ is consistent with the dilatometric data.

The electron micrographs in Figure IV.7 demonstrate reaustenitisation from $\alpha_a+\gamma$ at different isothermal transformation temperatures. Figure IV.7a shows the microscopy for reaustenitisation at 680°C for 10 minutes, in which the morphology of acicular ferrite is still clear but some austenite layers (now martensite) acquire protuberances. This indicates that the amount of austenite growth is very small. The micrograph of Figure IV.7b also presents austenite layer swelling towards ferrite in some area when specimen is reaustenitised at 700°C for 10 minutes. Figure IV.7c and d show the microstructures for reaustenitisation at 720°C, and 740°C for 2 hours. The volume fraction of austenite increases as the isothermal reaustenitisation temperature increases. Due to the smoothly

curved lenticular morphology of acicular ferrite, the austenite growth seems to involve the movement of a curved γ/α interface. It is also shown that the reaustenitisation completes at 760°C and above in Figure IV.7e and f.

4.2.3 Microanalysis

The microanalytical data (Table IV.1 and 2, Figure IV.8, 9 and 10) cover a range of times (t) and each $T_{\gamma'}$ and a range of isothermal reaustenitisation temperatures. The results for the two different starting microstructures $\alpha_b+\gamma$ and $\alpha_a+\gamma$ are generally not very different. They show that for low $T_{\gamma'}$ substitutional alloying additions redistribute during the $\alpha \rightarrow \gamma$ transformation, even at low t. For low transformation times, the degree of partitioning of alloying elements (as indicated by the deviation of the partition coefficient k_i from unity, where $k_i = X_i^{\gamma}/X_i^{\alpha}$) increases with decreasing $T_{\gamma'}$. This is consistent with the fact that at low $T_{\gamma'}$ the redistribution of substitutional alloying elements is a thermodynamic necessity [37,111]. As the driving force for reaustenitisation increases, the transformation tends toward paraequilibrium or negligible-partitioning-local equilibrium; this is illustrated clearly by the data for 760°C, even for times as short as 40 seconds and 2 minutes. In Figure IV.10a, the energy dispersive X-ray spectra show that for the specimen reaustenitised at 760°C for 40 seconds the ratio (atom fraction of Mn/atom fraction of Ni) is the same in the α and γ phases. However in Figure IV.10b, the energy dispersive X-ray spectra show that for the specimen reaustenitised at 680°C for 10 minutes the ratio is much higher than in γ than in α, even though the amount of reaustenitisation is quite small.

The concepts of paraequilibrium and local equilibrium have been reviewed in Section 1.5. Paraequilibrium is a state of constrained equilibrium in which the substitutional lattice is configurationally frozen with respect to the transformation interface. Hence, even though the transformation is diffusional in nature, the ratio (atom fraction of substitutional element i/atom fraction of iron) is the same in α and γ. Thus, the chemical potentials of the substitutional elements are not equal in the two phases. Carbon which diffuses faster reaches equilibrium subject to this constraint. In negligible-partitioning-local equilibrium (NPLE), equilibrium is maintained for all species at the transformation interface, but the concentration of substitutional element is essentially the same in all phases.

The results also show that as t increases for a given $T_{\gamma'}$ the partition coefficient k_i changes even though the volume fraction of austenite undergoes negligible change. This is strong evidence that the concentrations of alloying elements at the interface during the growth of austenite are not equilibrium concentrations.

These results are qualitatively consistent with the dilatometric data for both starting microstructures $\alpha_b+\gamma$ and $\alpha_a+\gamma$. One of the factors responsible for the increased rate of transformation at high T_γ is the fact that the degree of redistribution of alloying elements during transformation decreases with increasing T_γ. The results again emphasize that although the states of local equilibrium or paraequilibrium are for convenience often assumed to define the compositions at the interface during diffusion-controlled growth, an infinite number of other possibilities exist for multicomponent alloys [25]. All compositions of austenite which allow a reduction in free energy during growth can in principal form from ferrite, giving rise to situations in which one or more of the element is trapped by the moving interface; trapping implies an increase in the chemical potential of that element during transfer across the interface. The prediction of compositions at the interface is then a formidable theoretical problem which cannot be addressed until detailed information on interface mobility becomes available. On the other hand, any system must eventually tend towards equilibrium, so that the limiting composition of austenite can easily be calculated; this is the approach adopted in the present work.

4.3 Theoretical Analysis

In this section a thermodynamic model is presented for the interpretation of the observations on reaustenitisation from starting microstructure acicular plus austenite (or bainite plus austenite). Since after the diffusionless growth of acicular ferrite (bainite), carbon is rapidly and spontaneously redistributed into the residual austenite with an accompanying reduction in free energy, the $\alpha_a \rightarrow \gamma$ ($\alpha_b \rightarrow \gamma$) transformation in its original form is irreversible. The problem of reaustenitisation is therefore considerably different from the case of reverse transformation from martensite to austenite in for example, shape memory alloys.

It is noted that the formation of acicular ferrite (or bainite) ceases prematurely during isothermal transformation when the carbon content of the residual austenite reaches the T_o' curve (the phase diagram for the alloy is presented in Figure IV.11). It follows that the carbon concentration X_γ' of the austenite when the formation of acicular ferrite (or bainite) ceases at T_a, is given by (point marked a in Figure IV.11):

$$X_\gamma' = X_{T_o'}\{T_a\} \qquad \text{(IV/1)}$$

Furthermore, it is noted that:

$$X_\gamma' << X_{Ae_3}\{T_a\} \qquad \text{(IV.2)}$$

where $X_{Ae_3}\{T_a\}$ is marked b in Figure IV.11.

Thus, although the formation of acicular ferrite (or bainite) ceases at T_a, because $X'_\gamma << X_{Ae_3}\{T_a\}$, the driving force for austenite to transform diffusionally to ferrite is still negative. Another way of expressing this is to say that the volume fraction of acicular ferrite (or bainite) present when its formation ceases at T_a is much less than is required by the lever rule. In fact, this remains the case until the temperature T is high enough (i.e., $T = T_{\gamma 1}$) to satisfy the equation:

$$X'_\gamma = X_{Ae_3}\{T_a\} \qquad \text{(IV.3)}$$

Hence, reaustenitisation will first occur at a temperature $T_{\gamma 1}$, as indicated in Figure IV11 (marked C), and as observed experimentally. Note that this is a direct consequence of the mechanism of the acicular ferrite (bainite) transformation, which does not allow the transformation to reach completion. If this were not the case, then the lever rule demands that the temperature need only be raised infinitesimally above T_a in order for the reverse $\alpha \rightarrow \gamma$ transformation to be thermodynamically possible!

The theory goes further than explaining just the temperature at which the reverse transformation should begin. It also predicts that any temperature T_γ greater than $T_{\gamma 1}$, the reverse $\alpha \rightarrow \gamma$ transformation should cease as soon as the residual austenite carbon concentration X_γ (initially X'_γ) reaches the Ae_3 curve, i.e., when:

$$X_\gamma = X_{Ae_3}\{T_\gamma\} \qquad \text{(IV.4)}$$

with the equilibrium volume fraction of austenite (at the temperature T_γ), $V_\gamma\{T_\gamma\}$, being given by:

$$V_\gamma\{T_\gamma\} = \bar{X}/X_{Ae_3}\{T_\gamma\} \qquad \text{(IV.5)}$$

assuming that the carbon concentration of ferrite is negligible and $X_{Ae_3}\{T_\gamma\} > \bar{X}$ When $X_{Ae_3}\{T_\gamma\} = \bar{X}$, the alloy eventually becomes fully austenitic (point d, Figure IV.11) and if this condition is satisfied at $T_\gamma = T_{\gamma 2}$, then all $T_\gamma > T_{\gamma 2}$, the alloy transforms completely to austenite.

These concepts immediately explain the dilatometric data in which the degree of $\alpha \rightarrow \gamma$ transformation increase (from ≈ zero at 680°C) with the temperature of isothermal reaustenitisation, until the temperature 760°C = $T_{\gamma 2}$ where the alloy transforms completely to austenite. This theory has been applied using a computer program (in Appendix 1) to

convert the volume fraction of austenite to relative length change for isothermal reaustenitisation as shown in Figure IV.5, in which the calculated curves C and D assume that the α_a (or α_b) reaction stop at T_0 or T_0' curve of the phase diagram, respectively. The calculated results are very consistent with the experimental data.

4.4 Conclusions

Reaustenitisation of a weld deposit, beginning with a microstructure of just acicular ferrite plus austenite, or bainite plus austenite has been studied under isothermal conditions and in circumstances where the nucleation of austenite is not necessary. The same results of dilatometry and microanalysis for isothermal reaustenitisation from starting microstructures $\alpha_a+\gamma$ and $\alpha_b+\gamma$ have been obtained. Because acicular ferrite is in fact intragranular bainite, its mechanism of reaustenitisation is the same as that of bainite. It is found that the reverse transformation from acicular ferrite (or bainite) to austenite does not happen immediately when the temperature is raised (above that at which the acicular ferrite formed), even though the alloy is within the $\alpha+\gamma$ phase field. This is because acicular ferrite plates grow by a diffusionless displacive transformation mechanism (similar to that of bainite) which ensures that the transformation ceases prematurely, before the residual austenite achieves its equilibrium composition. Hence, reaustenitisation only occurs when the alloy is heated to a temperature (well above the Ae_1 temperature of the alloy) where the carbon concentration of the residual austenite exceeds its equilibrium concentration. Complete transformation to austenite only occurs at a temperature where the alloy composition equals the austenite equilibrium composition. However, at all intermediate temperatureures, the reverse $\alpha\rightarrow\gamma$ transformation terminates before the alloy becomes fully austenitic, with the volume fraction of austenite increasing isothermal reaustenitisation temperature.

In the case of a starting microstructure bainite plus austenite, the transmission electron micrographs show that the austenite layers become thicker and still remain parallel with each other as the reaustenitisation temperature increases. This provides strong evidence that austenite essentially grows by the movement of the planar γ/α interface. On the other hand, in the case of starting microstructure acicular ferrite plus austenite, owing to the non-parallel plate and smoothly curved morphology of acicular ferrite, the austenite growth seems to move a curved γ/α interface. The microanalytical date (for both $\alpha_a+\gamma$ and $\alpha_b+\gamma$) show that for low reaustenitisation temperatures, substitutional alloying elements redistribute during the $\alpha\rightarrow\gamma$ transformation, even in a very short period of time. The degree of redistribution of alloying elements during transformation decreases with increasing reaustenitisation temperature. Eventually the partition coefficients k_i for substitutional alloying elements equal unity, as the reaustenitisation temperature raises to

close the fully austenitic temperature. This implies that, as the driving force for reaustenitisation increases, the transformation tends toward paraequilibrium or negligible-partitioning-local equilibrium.

The work has led to a theory for reaustenitisation which explains most of the experimental results. The model predicts accurately the temperature at which reaustenitisation should begin and the degree of transformation to austenite as a function of the isothermal reaustenitisation temperature. All this is in turn a function of the temperature at which the original acicular ferrite (or bainite) itself formed.

(a)

(b)

Figure IV.1 - Effect of tempering on the precipitation of cementite.
(a) 10 mins @ 950°C → 30 mins @ 460°C → 30 mins @ 600°C
(b) 10 mins @ 950°C → 30 mins @ 460°C → 140 mins @ 600°C

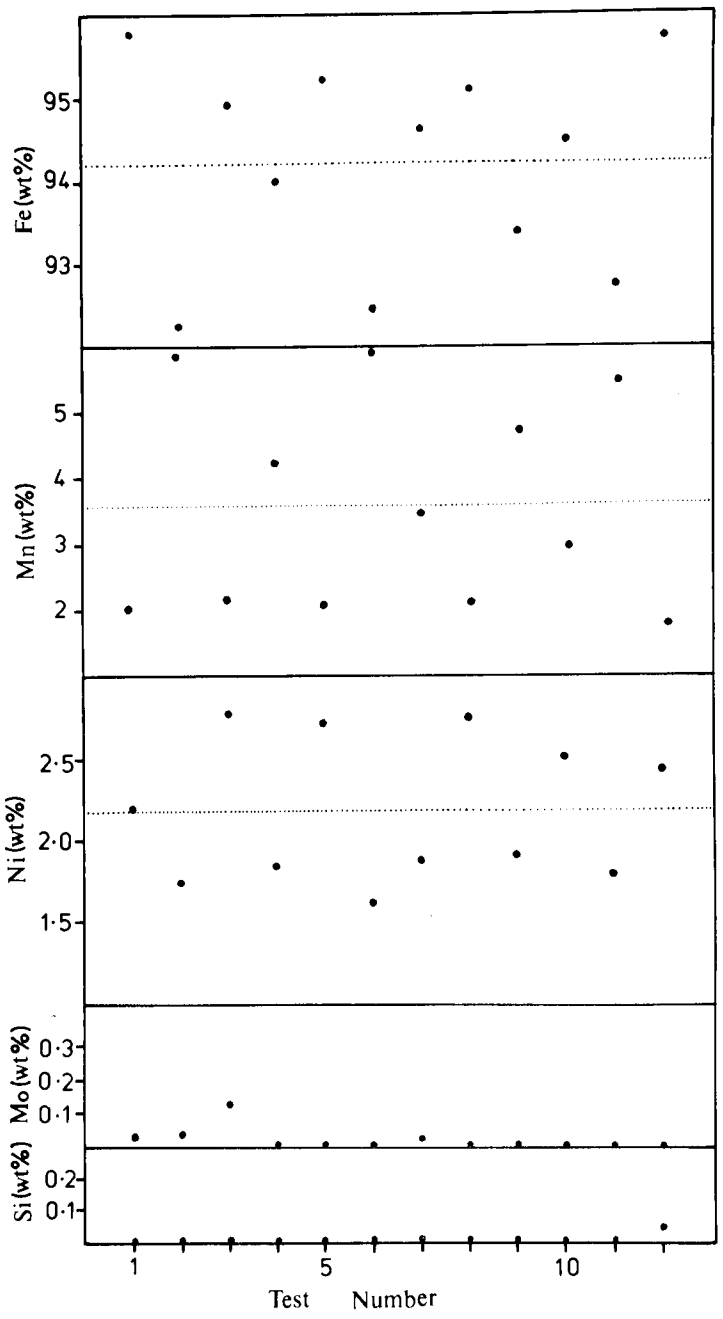

Figure IV.1(c) - Microanalytical data obtained using energy dispersive X-ray analysis on a Philips EM400T for cementite particles as shown in Figure IV.1(b).

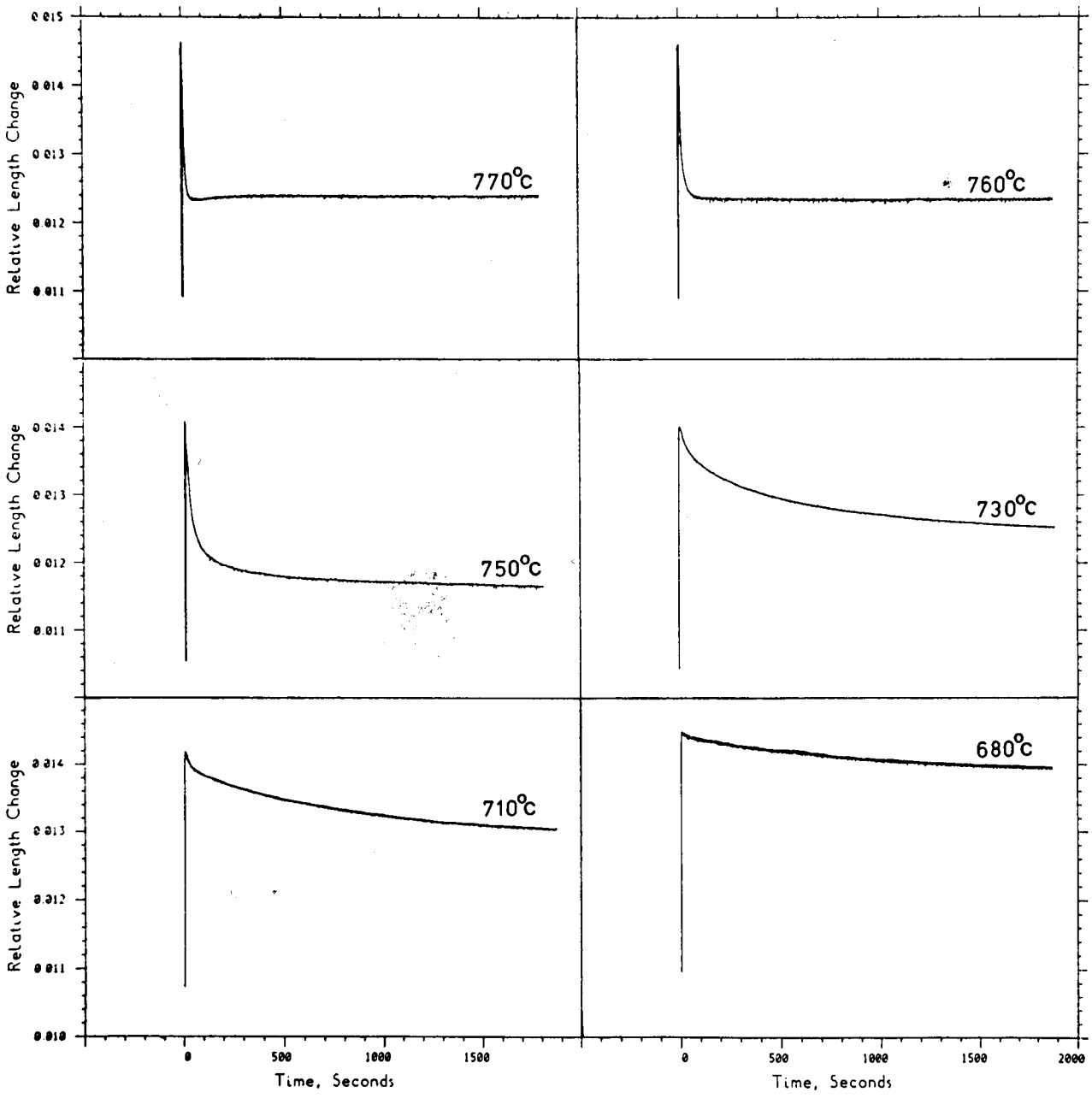

Figure IV.2 - Isothermal reaustenitisation using dilatometry. The specimens were initially austenitised at 950°C for 10 minutes, isothermally partially transformed to bainite at 460°C for 30 minutes and then rapidly up-quenched to an isothermal reaustenitisation temperature.

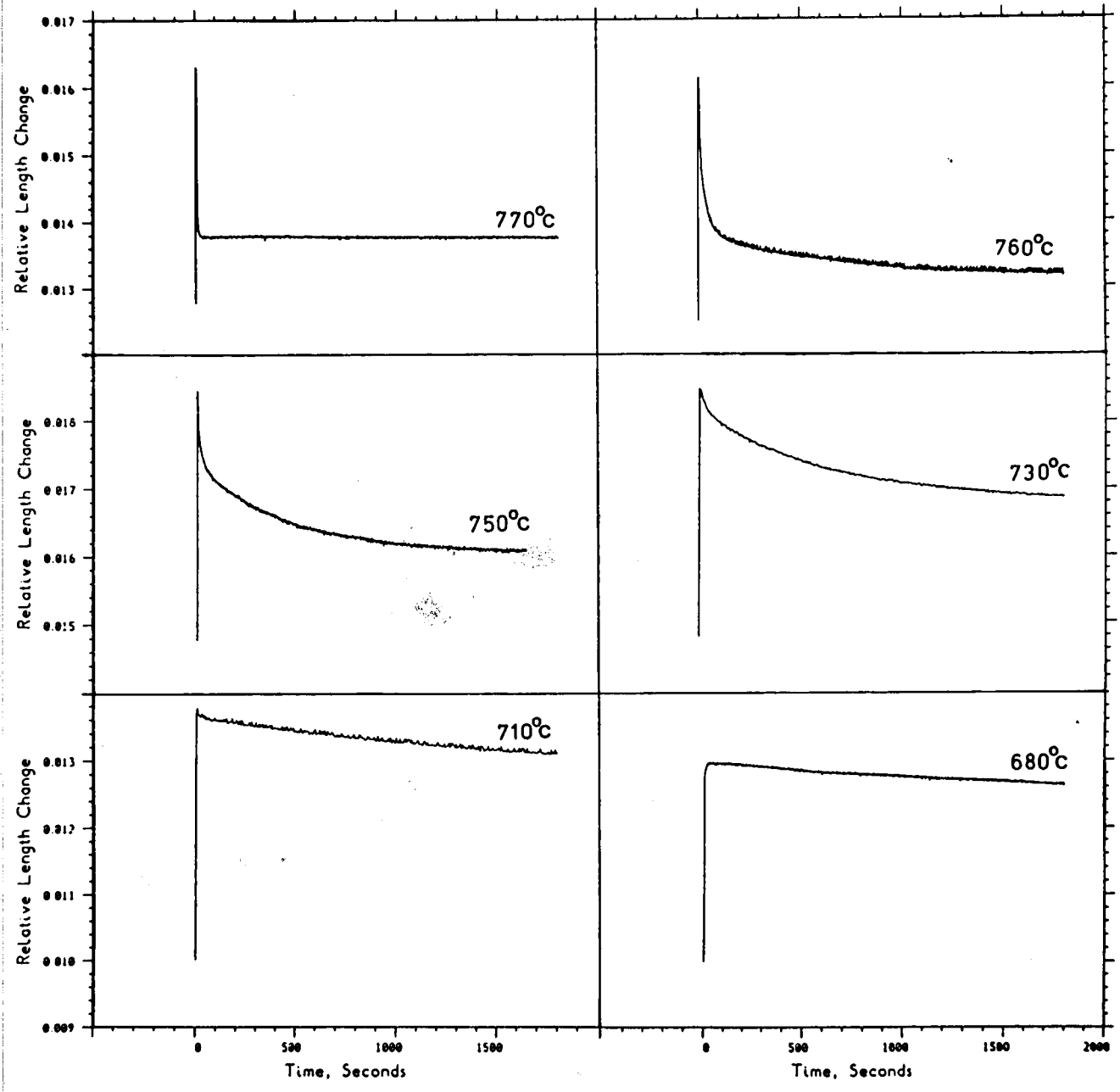

Figure IV.3 - Isothermal reaustenitisation using dilatometry. The specimens were initially at 1200°C for 30 minutes, isothermally partially transformed to acicular ferrite at 460°C for 30 minutes and then rapidly up-quenched to an isothermal reaustenite temperature.